Flexible and Porous Nanocellulose Aerogels with High Loadings of Metal-Organic Framework Particles for Separations Applications

He Zhu, Xuan Yang, Emily D. Cranston*, and Shiping Zhu*

DOI: 10.1002/adma.201601351

Submitted to ADVANCED MATERIALS
NaDOI: 10.1002/adma.((please add manuscript number))

Flexible and Porous Nanocellulose Aerogels with High Loadings of Metal-Organic Framework Particles for Separations Applications

By *He Zhu, Xuan Yang, Emily D. Cranston*, and Shiping Zhu**

[*] H. Zhu, X. Yang, Prof. E. D. Cranston, Prof. S. Zhu
Department of Chemical Engineering,
McMaster University, Hamilton,
Ontario, Canada, L8S 4L7
E-mail: ecranst@mcmaster.ca, zhuship@mcmaster.ca

Keywords: metal-organic frameworks • cellulose nanocrystals • aerogels • water purification • porous materials

This work overcomes the longstanding challenge of processing metal-organic framework (MOF) powders into a convenient and tailorable form by entrapping them within a cellulose nanocrystal (CNC) aerogel. MOFs are a new class of porous materials, assembled from metal ions or ion clusters bridged by organic ligands. Since the pioneering work on MOF-5 reported by Yaghi and co-workers,[1] MOFs have received great attention due to their large surface area and porosity, high thermal stability, and tunable pore structure. MOFs have shown great potential in various applications including gas separation[2] and storage,[3] chemical sensing,[4] catalysis,[5] and so on. Designing and preparing new MOFs,[6] post-modification of existing MOFs,[7] and fabrication of MOFs into different structures[8] are currently of great interest. However, due to the crystalline nature of MOFs, they are most commonly found in powder form and their processability and handling remain a significant challenge.[9] Integrating MOFs onto or within various substrates to produce a shapeable, cost-efficient, and chemically inert product is one way to expand the potential applications of these functional materials.

The deposition and growth of MOF particles on substrates has become a highly researched area but is severely constrained by the physical and chemical requirements of the substrate and gives materials with limited functionality.[10] Usually surface modifications are needed in

order to increase the compatibility between MOFs and substrates, and while different methods to grow MOFs exist, including solvothermal,[11] secondary,[12] layer by layer growth,[13] and electrochemical deposition,[14] the substrates have to be stable during the process or restricted synthetic conditions must be employed.[15] Incorporation of MOF particles onto polymer or fiber substrates (of both synthetic[16] and natural origin[17]), by blending, deposition or *in situ* growth, has been demonstrated. However, while these approaches overcome some of the disadvantages of preparing MOF-only materials or planar MOF films, most examples reported to date are either limited by low MOF loadings or reduced flexibility.[16b, 18] One alternative approach used to avoid processing or depositing MOFs is to produce metal organic framework gels (MOGs) which are high surface area MOF-like materials but they generally lack the ordered crystal lattice and desired physical properties of MOFs.[19]

Nanocellulose shows great promise for use as a supporting substrate[20] or templating material[21], especially in the form of cellulose aerogels and foams, because of its high strength, light weight, low cost, non-toxicity and its ability to be processed easily in water.[22] Cellulose nanocrystals (CNCs), cellulose nanofibrils (CNFs), and bacterial cellulose are the most common types of nanocellulose which are now being produced with consistency in industrial-scale quantities yet few commercial products exist.[23] Interestingly, CNCs and CNFs have been found to help unstable colloidal nanoparticles like carbon nanotubes (CNT), boron nitride, manganese dioxide or molybdenum disulfide suspend better in water.[20b, 24] Moreover, the co-suspended nanoparticles can be processed to give hybrid nanocomposites with uniform distribution of components.[20b] Only one literature example exists combining MOFs and nanocellulose; it is an elegant study of growing MOFs (up to 44 wt.% loading) *in situ* on CNFs and preparing a densely-packed film supported by filter paper for gas separations.[25] Due to the combination of amorphous and crystalline cellulose regions in CNFs, they are known to pack well, forming good barrier films with low oxygen permeability,

and when the MOFs were incorporated only gas molecules smaller than the MOF pores could penetrate the film.[25] In contrast, we use highly crystalline rigid rod-shaped CNC nanoparticles. When cross-linked together, the nanoparticles form highly porous self-supported 3D materials, which have tailorable absorbent and mechanical performance.[26]

Herein, we report a facile and novel method to combine functional MOFs and structural CNCs into a flexible and porous aerogel with hierarchical structure without the use of chemical modifiers. The hybrid materials are prepared through a straightforward sol-gel process, followed by freeze-drying. Three different MOF-containing aerogels are demonstrated with up to 50 wt.% of uniformly distributed MOFs. This new strategy is based on orthogonally functionalized celluloses, which individually form colloidally stable suspensions but assemble into covalently cross-linked clusters with entrapped MOFs, when mixed together. The combination of MOFs, cross-linked clusters and freeze drying, gives hybrid aerogels with hierarchical pores that remain intact in liquid under compression. MOFs retain their crystallinity, porosity and accessibility in the aerogel format making them ideal absorbents for water purification and other separations applications.

Hybrid MOF aerogels were prepared by mixing MOF particles with cross-linkable CNCs to form a stable colloidal suspension in water, and then added to an aqueous solution of cross-linkable carboxymethyl cellulose (CMC). More specifically, cross-linkable celluloses were based on aldehyde modified CNCs (CHO-CNCs) and hydrazide modified CMC ($NHNH_2$-CMC) which form hydrazone cross-links when in contact. The mixture thus contained cross-linked clusters composed of MOFs trapped in CNCs cross-linked to CMC, however these clusters remained colloidally stable. The suspension of clusters was frozen and freeze-dried to prepare the hybrid aerogels shown schematically in **Figure 1**A. Three MOF types with different sizes and functionalities were synthesized and successfully incorporated into the

cellulose aerogels, including zeolitic imidazolate framework-8 (ZIF-8),[27] University of Oslo-66 (UiO-66),[28] and Material Institute de Lavoisier-100(Fe) (MIL-100(Fe)).[29] The resultant hybrid aerogels were uniform, flexible, and could easily be handled without any loss of structural integrity (Figure 1B and Supporting Information Video S1). Powder X-ray diffraction (PXRD) of the aerogels showed that the MOF crystallinity was retained during the processing (Supporting Information Figure S1).

Similarly, hybrid aerogels were prepared without CMC such that the substrate was entirely composed of orthogonally functionalized CNC nanoparticles (i.e., CHO-CNCs and $NHNH_2$-CNCs).[26b] However, when high loadings of MOFs were used the hybrid aerogels exhibited a more loosely connected structure and fell apart easily (Figure 1C). As the MOF particles and CNCs are both rigid crystalline structures we believe that the ability to form CNC-CNC cross-links is sterically hindered in this system and thus the flexible $NHNH_2$-CMC is needed to gives aerogels with robust mechanical behavior.

The loading of MOF particles within the cellulose aerogels can be controlled by tuning the ratio of the three components in the initial suspensions. UiO-66-containing aerogels were chosen as an example to investigate the effect of MOF loading on the aerogel morphology and performance. We achieved loadings as high as 50 wt.%, above which the clusters are no longer stable in suspension and cannot be processed by the sol-gel method. Aerogels with 20, 33.3, and 50 wt.% UiO-66 added were prepared and characterized by thermogravimetric analysis (TGA) and scanning electron microscopy (SEM). The UiO-66 loadings determined by TGA were consistent with the nominal values indicating that all MOFs added to the suspension were incorporated into the aerogel (Supporting Information Table S1). The hybrid aerogels had ultralow densities, increasing slightly with MOF loading from 18.4 ± 0.2 mg/cm^3 for 20 wt.% to 22 ± 1 mg/cm^3 and 32.8 ± 0.4 mg/cm^3 for 33.3 and 50 wt.% MOFs,

respectively. This implies that we have significant control over the MOF loading and density and that the aerogels are extremely porous with a large accessible surface area.

The morphology of these hybrid aerogels was studied by SEM to investigate the hierarchical structure (**Figure 2**). In general, all aerogels exhibit a similar internal pore structure, consisting of micro pores from the well-defined MOF pores (not visible by SEM), meso pores between the cross-linked CNCs and CMC which make up the "walls" of the structure, and macro pores templated from the ice crystals that grow when the suspension of clusters is frozen. Additionally, MOF particles are well dispersed within the "walls" and no MOF agglomerates are observed. We believe this uniformity stems from the ability for CNCs to aid in the suspension of MOF particles and the regularity in the cross-linked clusters, highlighting the intricacies of our processing method. The versatility of the approach is also confirmed through the preparation of aerogels with ZIF-8 and MIL-100(Fe) which exhibit similar morphology (Supporting Information Figure S2).

At low MOF loadings, macroscopic regions without any MOFs are observed in the mesoporous "walls" of the aerogels (Figure 2A and 2B); however, at high MOF loadings, the "walls" are predominantly MOF particles (Figures 2E and 2F). Importantly, the MOFs appear entrapped within the cellulose matrix and are not merely attached to the surface (Figure 2F). This structure is predicted to minimize MOF loss and leaching during use, as tested below. The high MOF loading achieved and the porous structure of the aerogel indicate that we have produced a novel hybrid material, which retains the favourable properties of both MOFs and CNCs. We expect that the morphology of the aerogels has led to one of the highest surface-area accessible and lightweight MOF-containing materials reported to date. While MOF-only powders/films are known to have higher surface areas than hybrid materials, they are difficult to process into useful forms.

Although MOFs are intended for various applications, here we test the water purification abilities of our hybrid aerogels to demonstrate that the MOFs are still functional when entrapped in the cellulose matrix. This is a particularly promising application area for this type of material as CNC aerogels are recognized to function as absorbents and can take up more than 100 times their own mass in water, be compressed to remove the liquid and re-used.[26b] Specifically we looked at using the UiO-66-containing aerogels to remove the hazardous compound potassium dichromate, which is the most toxic form of chromium, Cr(VI), which often ends up in water streams due to industrial pollution.[30] In the test, a small aerogel (~0.8 cm^3) was placed into 10 mL of an aqueous solution containing 10 mg/L potassium dichromate. The Cr(VI) contaminated water was initially light yellow but became colorless after the hybrid aerogel adsorbed the contaminants, while conversely the color of the hybrid aerogel itself changed from white to light yellow (**Figure 3**A). This color change due to water purification was even more striking in the case of MIL-100(Fe)-containing aerogels which removed Rhodamine B (Supporting Information Figure S3).

The adsorptive capacities (q_t in mg/g) of the MOF particles within the aerogels at different times (t) were obtained to study the kinetic behavior (see Experimental Section for details). The time-dependence of the adsorption was well-fitted to a pseudo-second-order kinetic model with rate constant k_2 (Figure 3B and Supporting Information Figure S4) which is the expected diffusion limited behavior of MOFs and implies that the cellulose support is not hindering the accessibility of the MOF pores. The values of the kinetic parameters are summarized in the Supporting Information Table S2. The aerogel containing 50 wt.% UiO-66 adsorbed 85% of the Cr(VI) after 24 hours, while aerogels with lower MOF loadings adsorbed 67% (33.3 wt.% UiO-66) and 51% (20 wt.% UiO-66) of the Cr(VI) due to the lower MOF content. Aerogels without MOFs (control sample) did not show any removal of Cr(VI) after

24 hours according to UV-Vis spectroscopy. No MOF particles were released from the aerogels into the water after 24 hours of soaking as tested by dynamic light scattering (DLS) and similarly, no breakdown of MOFs or leaching was detected by inductively coupled plasma optical emission spectrometry (ICP-OES) testing for trace Zr content (Supporting Information Table S3).

The adsorption capacity of pure UiO-66 powder was also tested to compare with the MOF-containing aerogels. When the same mass of MOF powder as was present in the aerogel was used, the powder was found to adsorb 85% of the Cr(VI) after 24 hours, which is the same as the corresponding hybrid aerogel. However, if the total mass of the aerogel is considered then the mass specific adsorption capacity is slightly lower for the aerogels. In all cases, equivalent or superior adsorption capacity (based on mass of MOFs) was observed for the aerogels (**Table 1**), indicating that all of the MOF particles within the aerogel are functional. We believe the aerogel's hierarchical porous structure contributes significantly to this good performance where the combination of easy accessibility through macropores, and capillary effect of mesopores, allow for fast water uptake and contact between the MOF micropores and the contaminants.

In addition to adsorbing large amounts of contaminants, the aerogels could be compressed to squeeze out the water, which always contained a lower concentration of contaminants than the bulk solution; for example, in one test, after 8 hours of soaking, the concentration of Cr(VI) within the aerogel (with 50 wt.% UiO-66) was 1.8 mg/L while the bulk solution had a concentration of 3.7 mg/L. This concentration difference contributed to the aerogel performance by consistently driving more contaminated water into the aerogel until saturation. Additionally, no leaching of MOF particles occurred during the compression process since no particle signal was detected by DLS. The compressed aerogels quickly recovered their shape

when re-immersed in water (Figure 3C). Hybrid aerogels with ZIF-8 and MIL-100 were also tested for water treatment and showed a high capacity for the removal of other hazardous materials including benzotriazole and Rhodamine B, for ZIF-8 and for MIL-100(Fe) aerogels, respectively (Supporting Information Figure S3 and Table S2).

In conclusion, we have demonstrated a facile way of combining two emerging materials – MOFs and CNCs – into one highly functional aerogel. The CNCs act as the structural component supporting the functional MOFs in a three dimensional flexible and lightweight networked material. The MOF loading can be tailored by changing the initial ratio of components, up to 50 wt.% MOF content can be easily achieved. Three different types of MOFs were embedded into the CNC-based aerogels, highlighting the versatility of the processing method and materials, and showing that the MOFs retain their crystallinity and function. Water treatment applications were demonstrated based on the good absorption properties of aerogels, however these materials may also be extended to be used as air filters, substrate-supported catalysis, and sensors, to name just a few examples.

Experimental

Materials. Whatman cotton ashless filter aid was purchased from GE Healthcare Canada, and sulfuric acid (95−98%) was purchased from VWR Canada. Dimethyl sulfoxide (DMSO, reagent grade) was purchased from Caledon Laboratory Chemicals (Georgetown, ON, Canada). Sodium carboxmethyl cellulose (CMC, Mw ~ 250000 g/mol, DS = 0.9), adipic acid dihydrazide (ADH, 98%), N-hydroxysuccinimide (NHS, 97%), N'-ethyl-N-(3-dimethylaminopropyl)-carbodiimide (EDC, commercial grade), zinc nitrate hexahydrate (98%), 2-methylimidazole (99%), zirconium chloride (≥99.5%), terephthalic acid (BDC, 98%), acetate acid (≥99.7%), iron (III) chloride hexahydrate (≥98%), trimethyl 1,3,5-

benzenetricarboxylate (95%), benzotriazole (99%), potassium dichromate (≥99%), and Rhodamine B (≥95%) were purchased from Sigma-Aldrich and used without further purification. All water used was purified Type I water with a resistivity of 18.2 MΩ· cm (Barnstead NANOpure DIamond system, Thermo Scientific, Asheville, NC).

MOFs. ZIF-8 (Zeolitic Imidazolate Framework-8), UiO-66 (University of Oslo-66), and MIL-100(Fe) (Material Institute de Lavoisier-100(Fe)) were prepared using the methods reported in the literatures [31]. Briefly, ZIF-8 was prepared by dropping zinc nitrate solution (1.17 g zinc nitrate hexahydrate in 8 g water) into 2-methylimidazole solution (22.7 g 2-methylimidazole in 80 g water) under stirring for 10 minutes and collected by ultracentrifugation and washed 3 times with water. UiO-66 was prepared by dissolving zirconium chloride (915 mg) and BDC (645 mg) in 225 mL DMF containing 6.7 mL acetic acid, which was kept under 120 °C for 24 hours and collected by centrifugation and washed with methanol (3 times) afterwards. MIL-100(Fe) was prepared by dispersing iron (III) chloride hexahydrate (0.162 g) and trimethyl 1,3,5-benzenetricarboxylate (0.138 g) in 5 mL water, which was then kept under 130 °C for 3 days. The product was centrifuged and washed with acetone (3 times).

Preparation of Carboxymethyl Cellulose-Hydrazide ($NHNH_2$-CMC), Hydrazide-Modified CNCs ($NHNH_2$-CNCs) and Aldehyde-Modified CNCs (CHO-CNCs). $NHNH_2$-CNCs and CHO-CNCs were synthesized using the method described in our previous work [26a]. Briefly, hydrazide groups were introduced onto CMC (or CNC) by reacting ADH with CMC (or CNC) through the NHS/EDC coupling system; aldehyde groups were generated by the oxidization of the CNC using $NaIO_4$. Solutions/suspensions were stored at 4 °C before further experiments.

Preparation of Hybrid Aerogels. MOF nanoparticles were suspended into 1 wt.% CHO-CNC suspensions, with 15 min of probe sonication. The resulting suspensions were mixed with an equal volume of 1 wt.% $NHNH_2$-CMC, or $NHNH_2$-CNCs, using a vortex mixer (Level 8, Analog Vortex Mixer, VWR) for 2 min. The final suspension of cross-linked clusters was transferred into a cylindrical glass vial (14.5 mm in diameter) and allowed to set for another 10 min before transfer into the freezer (-20°C). The final hybrid aerogels were obtained by freeze-drying the ice-gel.

Adsorption. Adsorption kinetics were studied by soaking the aerogels or MOF particles in 10 mL aqueous solution containing different contaminants (200 mg/L benzotriazole for ZIF-8, 10 mg/L potassium dichromate for UiO-66, and 0.01 mM Rhodamine B for MIL-100(Fe)) for a predetermined time. Then the solution was analyzed by UV-Vis to determine the concentration based on a calibration curve prepared from solutions with known contaminant concentrations. The adsorption capacity at time t was calculated using the following equation:

$$q_t = \frac{(C_0 - C_t)V}{m}$$

where V is the solution volume, m is the mass of the aerogel or the mass of MOF particles, C_0 is the initial concentration, C_t is the concentration at time t. The time-dependence of the adsorption was fitted with the pseudo-second-order kinetic model, which is:

$$\frac{t}{q_t} = \frac{1}{k_2 q_e^2} + \frac{1}{q_e} t$$

where q_t and q_e are the adsorption capacities at time t and equilibrium, respectively, and k_2 is the rate constant of the pseudo-second-order model.

Characterization. JEOL JSM 7000 Scanning Electron Microscopy (SEM) was used to characterize the MOF particles and aerogels with a 5 nm platinum coating. Powder X-ray diffraction (PXRD) was conducted on a Bruker D8 Advance X-Ray Diffractometer with a

scan speed of 1 deg/min, a step size of 0.05°, and a 2θ range of 2-50°. The concentration of the contaminated water was determined by DU 800 UV/Vis Spectrophotometer. MOF nanoparticle size and the presence of MOFs in purified water test (leaching) were determined using a Malvern Zetasizer Nanoparticle Analyzer (dynamic light scattering apparatus) at 25 °C. Thermogravimetric analysis (TGA) was performed on a TA Q5000 thermogravimetric analyzer with a ramp rate of 10 °C/min. Inductively coupled plasma optical emission spectrometry (ICP-OES) was conduceted on Varian ICP-OES Vista Pro.

Acknowledgements
The authors thank Professors R. Pelton and A. Guarné for access to equipment, and Dr. G. de Silveira for training. This work was carried out using instruments in the Biointerfaces Institute and the Canadian Centre for Electron Microscopy. We sincerely thank the Natural Sciences and Engineering Research Council (NSERC) of Canada and the Canada Research Chair (CRC) program of the Federal Government for supporting this research.

Received: ((will be filled in by the editorial staff))
Revised: ((will be filled in by the editorial staff))
Published online: ((will be filled in by the editorial staff))

[1] H. Li, M. Eddaoudi, M. O'Keeffe, O. M. Yaghi, *Nature* **1999**, *402*, 276-279.
[2] a) H. T. Kwon, H.-K. Jeong, *Journal of the American Chemical Society* **2013**, *135*, 10763-10768; b) H. Zhu, H. Liu, I. Zhitomirsky, S. Zhu, *Materials Letters* **2015**, *142*, 19-22.
[3] a) A. R. Millward, O. M. Yaghi, *Journal of the American Chemical Society* **2005**, *127*, 17998-17999; b) X. Wang, L. Xie, K.-W. Huang, Z. Lai, *Chemical Communications* **2015**, *51*, 7610-7613.
[4] a) G. Lu, J. T. Hupp, *Journal of the American Chemical Society* **2010**, *132*, 7832-7833; b) J. Liu, F. Sun, F. Zhang, Z. Wang, R. Zhang, C. Wang, S. Qiu, *Journal of Materials Chemistry* **2011**, *21*, 3775-3778.
[5] a) M. J. Katz, S.-Y. Moon, J. E. Mondloch, M. H. Beyzavi, C. J. Stephenson, J. T. Hupp, O. K. Farha, *Chemical Science* **2015**, *6*, 2286-2291; b) J. E. Mondloch, M. J. Katz, W. C. Isley III, P. Ghosh, P. Liao, W. Bury, G. W. Wagner, M. G. Hall, J. B. DeCoste, G. W. Peterson, *Nature materials* **2015**.
[6] a) L. Cooper, T. Hidalgo, M. Gorman, T. Lozano-Fernández, R. Simón-Vázquez, C. Olivier, N. Guillou, C. Serre, C. Martineau, F. Taulelle, *Chemical Communications* **2015**, *51*, 5848-5851; b) E.-L. Zhou, P. Huang, C. Qin, K.-Z. Shao, Z.-M. Su, *Journal of Materials Chemistry A* **2015**, *3*, 7224-7228; c) A. K. Crane, B. O. Patrick, M. J. MacLachlan, *Dalton Transactions* **2013**, *42*, 8026-8033.
[7] a) M. Kim, J. F. Cahill, Y. Su, K. A. Prather, S. M. Cohen, *Chemical Science* **2012**, *3*, 126-130; b) H. Liu, H. Zhu, S. Zhu, *Macromolecular Materials and Engineering* **2015**, *300*, 191-197.
[8] a) N. Yanai, M. Sindoro, J. Yan, S. Granick, *Journal of the American Chemical Society* **2012**, *135*, 34-37; b) M. Pang, A. J. Cairns, Y. Liu, Y. Belmabkhout, H. C. Zeng, M. Eddaoudi, *Journal of the American Chemical Society* **2013**, *135*, 10234-10237; c) H. Zhu, Q. Zhang, S. Zhu, *Dalton Transactions* **2015**.
[9] S. Furukawa, J. Reboul, S. Diring, K. Sumida, S. Kitagawa, *Chemical Society Reviews* **2014**, *43*, 5700-5734.
[10] a) A. Bétard, R. A. Fischer, *Chemical reviews* **2011**, *112*, 1055-1083; b) S. Qiu, M. Xue, G. Zhu, *Chemical Society Reviews* **2014**, *43*, 6116-6140.
[11] a) S. Hermes, M. K. Schröter, R. Schmid, L. Khodeir, M. Muhler, A. Tissler, R. W. Fischer, R. A. Fischer, *Angewandte Chemie International Edition* **2005**, *44*, 6237-6241; b) H. Zhu, S. Zhu, *The Canadian Journal of Chemical Engineering* **2015**, *93*, 63-67.
[12] a) K. Tao, L. Cao, Y. Lin, C. Kong, L. Chen, *Journal of Materials Chemistry A* **2013**, *1*, 13046-13049; b) D. Liu, X. Ma, H. Xi, Y. Lin, *Journal of Membrane Science* **2014**, *451*, 85-93.
[13] a) O. Shekhah, H. Wang, S. Kowarik, F. Schreiber, M. Paulus, M. Tolan, C. Sternemann, F. Evers, D. Zacher, R. A. Fischer, *Journal of the American Chemical Society* **2007**, *129*, 15118-15119; b) O. Shekhah, R. Swaidan, Y. Belmabkhout, M. du Plessis, T. Jacobs, L. J. Barbour, I. Pinnau, M. Eddaoudi, *Chemical Communications* **2014**, *50*, 2089-2092.
[14] a) M. Li, M. Dincă, *Chemical Science* **2014**, *5*, 107-111; b) I. Stassen, M. Styles, T. Van Assche, N. Campagnol, J. Fransaer, J. Denayer, J.-C. Tan, P. Falcaro, D. De Vos, R. Ameloot, *Chemistry of Materials* **2015**, *27*, 1801-1807.
[15] a) N. Stock, S. Biswas, *Chemical reviews* **2011**, *112*, 933-969; b) M. S. Denny, S. M. Cohen, *Angewandte Chemie International Edition* **2015**, *54*, 9029-9032.
[16] a) H. Yehia, T. Pisklak, J. Ferraris, K. Balkus, I. Musselman, in *ABSTRACTS OF PAPERS OF THE AMERICAN CHEMICAL SOCIETY, Vol. 227*, AMER CHEMICAL SOC 1155 16TH ST, NW, WASHINGTON, DC 20036 USA, **2004**, pp. U351-U351; b) T. Rodenas, M. van Dalen, E. García‐Pérez, P. Serra‐Crespo, B. Zornoza, F.

Kapteijn, J. Gascon, *Advanced Functional Materials* **2014**, *24*, 249-256; c) M. G. Schwab, I. Senkovska, M. Rose, M. Koch, J. Pahnke, G. Jonschker, S. Kaskel, *Advanced Engineering Materials* **2008**, *10*, 1151-1155; d) M. Rose, B. Boehringer, M. Jolly, R. Fischer, S. Kaskel, *Advanced Engineering Materials* **2011**, *13*, 356-360; e) Y.-n. Wu, F. Li, H. Liu, W. Zhu, M. Teng, Y. Jiang, W. Li, D. Xu, D. He, P. Hannam, *Journal of Materials Chemistry* **2012**, *22*, 16971-16978.

[17] a) D. Wisser, F. M. Wisser, S. Raschke, N. Klein, M. Leistner, J. Grothe, E. Brunner, S. Kaskel, *Angewandte Chemie International Edition* **2015**, *54*, 12588-12591; b) P. Küsgens, S. Siegle, S. Kaskel, *Advanced Engineering Materials* **2009**, *11*, 93-95; c) A. R. Abbasi, K. Akhbari, A. Morsali, *Ultrasonics sonochemistry* **2012**, *19*, 846-852; d) M. da Silva Pinto, C. A. Sierra-Avila, J. P. Hinestroza, *Cellulose* **2012**, *19*, 1771-1779; e) E. López‐Maya, C. Montoro, L. M. Rodríguez‐Albelo, S. D. Aznar Cervantes, A. A. Lozano‐Pérez, J. L. Cenís, E. Barea, J. A. Navarro, *Angewandte Chemie International Edition* **2015**.

[18] a) K. Díaz, M. López-González, L. F. del Castillo, E. Riande, *Journal of Membrane Science* **2011**, *383*, 206-213; b) T. Rodenas, I. Luz, G. Prieto, B. Seoane, H. Miro, A. Corma, F. Kapteijn, F. X. L. i Xamena, J. Gascon, *Nature materials* **2015**, *14*, 48-55; c) S. Hwang, W. S. Chi, S. J. Lee, S. H. Im, J. H. Kim, J. Kim, *Journal of Membrane Science* **2015**, *480*, 11-19.

[19] a) M. R. Lohe, M. Rose, S. Kaskel, *Chemical Communications* **2009**, 6056-6058; b) L. Li, S. Xiang, S. Cao, J. Zhang, G. Ouyang, L. Chen, C.-Y. Su, *Nature communications* **2013**, *4*, 1774.

[20] a) M. Hamedi, E. Karabulut, A. Marais, A. Herland, G. Nyström, L. Wågberg, *Angewandte Chemie International Edition* **2013**, *52*, 12038-12042; b) X. Yang, K. Shi, I. Zhitomirsky, E. D. Cranston, *Advanced Materials* **2015**, *27*, 6104-6109; c) M. Kaushik, A. Moores, *Green Chemistry* **2016**.

[21] a) K. E. Shopsowitz, H. Qi, W. Y. Hamad, M. J. MacLachlan, *Nature* **2010**, *468*, 422-425; b) K. E. Shopsowitz, W. Y. Hamad, M. J. MacLachlan, *Angewandte Chemie International Edition* **2011**, *50*, 10991-10995; c) M. Giese, L. K. Blusch, M. K. Khan, W. Y. Hamad, M. J. MacLachlan, *Angewandte Chemie International Edition* **2014**, *53*, 8880-8884.

[22] a) R. J. Moon, A. Martini, J. Nairn, J. Simonsen, J. Youngblood, *Chemical Society Reviews* **2011**, *40*, 3941-3994; b) M. Roman, *Industrial Biotechnology* **2015**, *11*, 25-33.

[23] D. Klemm, F. Kramer, S. Moritz, T. Lindström, M. Ankerfors, D. Gray, A. Dorris, *Angewandte Chemie International Edition* **2011**, *50*, 5438-5466.

[24] a) M. M. Hamedi, A. Hajian, A. B. Fall, K. Håkansson, M. Salajkova, F. Lundell, L. Wågberg, L. A. Berglund, *ACS nano* **2014**, *8*, 2467-2476; b) Y. Li, H. Zhu, F. Shen, J. Wan, S. Lacey, Z. Fang, H. Dai, L. Hu, *Nano Energy* **2015**, *13*, 346-354.

[25] M. Matsumoto, T. Kitaoka, *Advanced Materials* **2015**, n/a-n/a.

[26] a) X. Yang, E. Bakaic, T. Hoare, E. D. Cranston, *Biomacromolecules* **2013**, *14*, 4447-4455; b) X. Yang, E. D. Cranston, *Chemistry of Materials* **2014**, *26*, 6016-6025.

[27] K. S. Park, Z. Ni, A. P. Côté, J. Y. Choi, R. Huang, F. J. Uribe-Romo, H. K. Chae, M. O'Keeffe, O. M. Yaghi, *Proceedings of the National Academy of Sciences* **2006**, *103*, 10186-10191.

[28] J. H. Cavka, S. Jakobsen, U. Olsbye, N. Guillou, C. Lamberti, S. Bordiga, K. P. Lillerud, *Journal of the American Chemical Society* **2008**, *130*, 13850-13851.

[29] P. Horcajada, S. Surblé, C. Serre, D.-Y. Hong, Y.-K. Seo, J.-S. Chang, J.-M. Greneche, I. Margiolaki, G. Férey, *Chemical Communications* **2007**, 2820-2822.

[30] a) R. Ramos, A. Martinez, R. Coronado, *Water Science and Technology* **1994**, *30*, 191-197; b) H. Daraei, A. Mittal, J. Mittal, H. Kamali, *Desalination and Water Treatment* **2014**, *52*, 1307-1315.

[31] a) Y. Pan, Y. Liu, G. Zeng, L. Zhao, Z. Lai, *Chemical Communications* **2011**, *47*, 2071-2073; b) R. Canioni, C. Roch-Marchal, F. Sécheresse, P. Horcajada, C. Serre, M. Hardi-Dan, G. Férey, J.-M. Greneche, F. Lefebvre, J.-S. Chang, *Journal of Materials Chemistry* **2011**, *21*, 1226-1233; c) G. Lu, C. Cui, W. Zhang, Y. Liu, F. Huo, *Chem. Asian J* **2013**, *8*, 69-72.

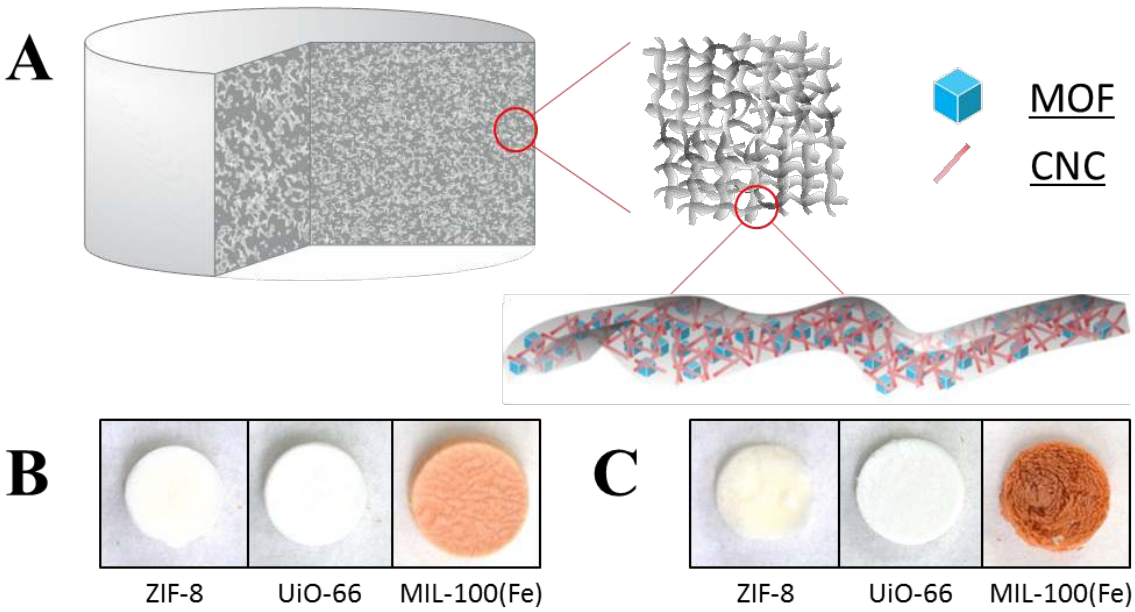

Figure 1. (A) Schematic of MOF-cellulose hybrid aerogel. Photographs of (B) CNC-CMC based hybrid aerogels (CNC:CMC:MOF=1:1:1 by weight), and (C) all-CNC based hybrid aerogels (CNC:CNC:MOF=1:1:1 by weight); aerogels are about 7 mm in diameter and 5 mm in height.

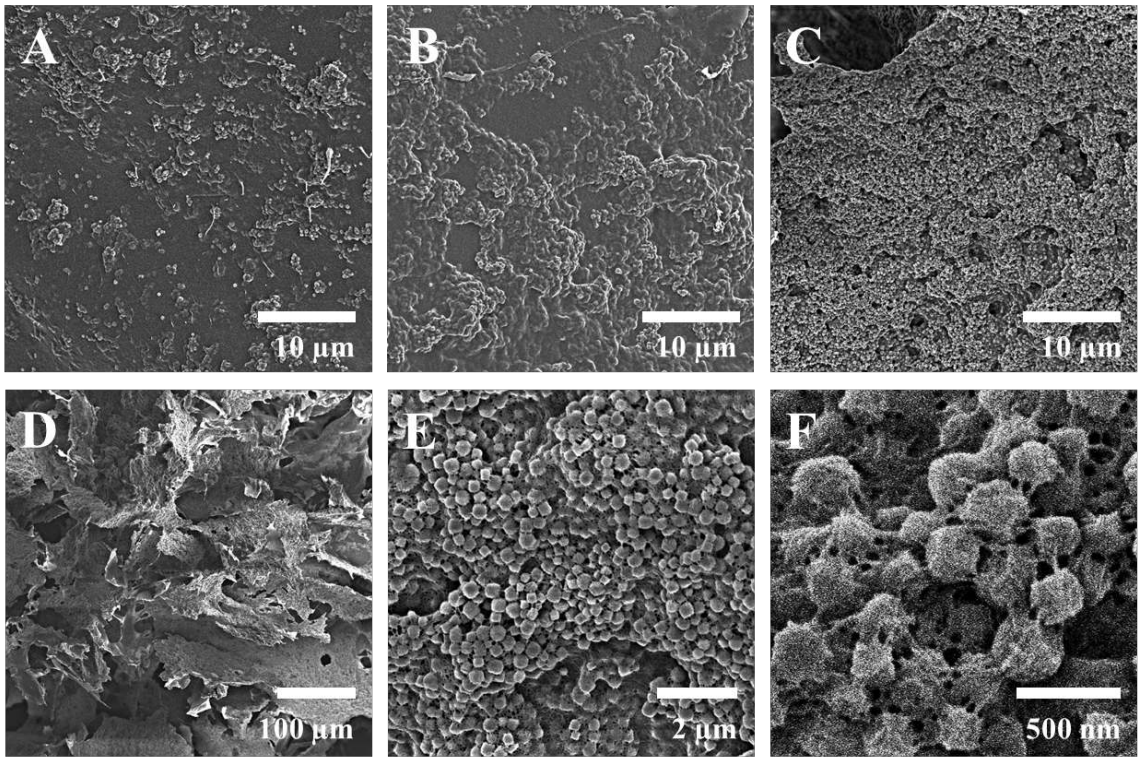

Figure 2. SEM images of UiO-66-containing cellulose aerogels. (A) Aerogel with 20 wt.% UiO-66, (B) aerogel with 33.3 wt.% UiO-66, (C, D, E, F) aerogels with 50 wt.% UiO-66 at different magnifications.

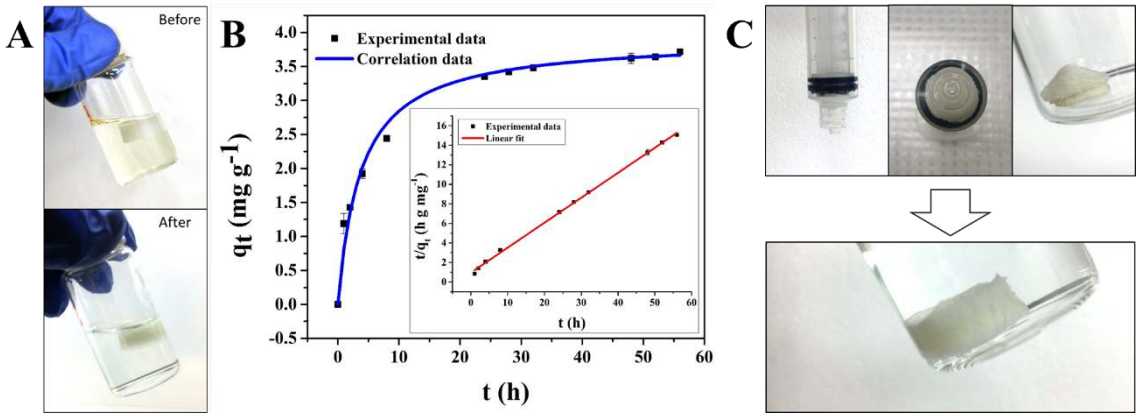

Figure 3. (A) Photographs of the contaminated aqueous solution before and after adsorbing Cr(VI) in the aerogel with 50 wt.% UiO-66 and (B) the time dependent adsorption (correlation curve was drawn using the kinetic parameters calculated from the pseudo-second-order model) and pseudo-second-order plots (inset). (C) Photographs showing that a wet hybrid aerogels (50 wt.% UiO-66) can be incorporated into a syringe and compressed fully by the piston (top left), also shown from the bottom view of the syringe (top middle). When removed from the syringe, the compressed aerogel in air maintains the shape of the container it was compressed in (top right) but recovers its original shape completely when place in solution again (bottom), this is also demonstrated in the Supporting Information Video S1.

Table 1. Adsorption capacities of Cr(VI) for aerogel with UiO-66, UiO-66 portion of aerogel, and UiO-66 powder.[a]

UiO-66 loading	Adsorption capacity q_t (mg g^{-1})[b]		
	Aerogel with MOF	MOF portion of aerogel[c]	MOF powder
20 wt.%	3.60	18.02	15.50
33.3 wt.%	3.89	11.66	8.40
50 wt.%	3.35	6.70	6.96

[a] The amount of the UiO-66 powder used for characterizing adsorption capacity was the same as the amount of the UiO-66 powder trapped within the aerogel. [b] The adsorption was conducted over 24 hours without any agitation. [c] This capacity was calculated with the same data used for the aerogel with MOF, but only the UiO-66 mass was used instead of the total aerogel mass.

The table of contents entry: Flexible and porous aerogels are obtained by combining functional MOFs and structural CNCs via a straightforward water-based sol-gel process, followed by freeze-drying. The aerogels have a hierarchical porous structure with controllable MOF loading up to 50 wt.%. These hybrid materials can be used as absorbents for water purification.

Keyword: metal-organic frameworks • cellulose nanocrystals • aerogels • water purification • porous materials

He Zhu, Xuan Yang, Emily D. Cranston*, and Shiping Zhu*

Flexible and Porous Nanocellulose Aerogels with High Loadings of Metal-Organic Framework Particles for Separations Applications

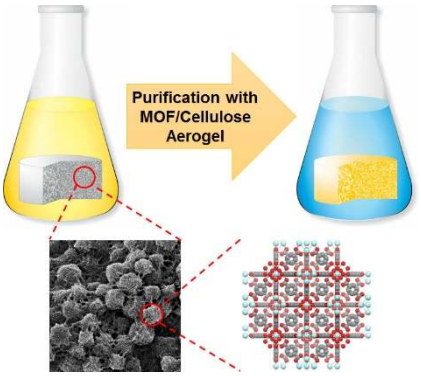

Submitted to ADVANCED MATERIALS

Supporting Information

Flexible and Porous Nanocellulose Aerogels with High Loadings of Metal-Organic Framework Particles for Separations Applications

He Zhu, Xuan Yang, Emily D. Cranston*, and Shiping Zhu*

Department of Chemical Engineering, McMaster University,
Hamilton, Ontario, Canada, L8S 4L7

* To whom correspondence should be addressed:
E-mail: ecranst@mcmaster.ca, zhuship@mcmaster.ca

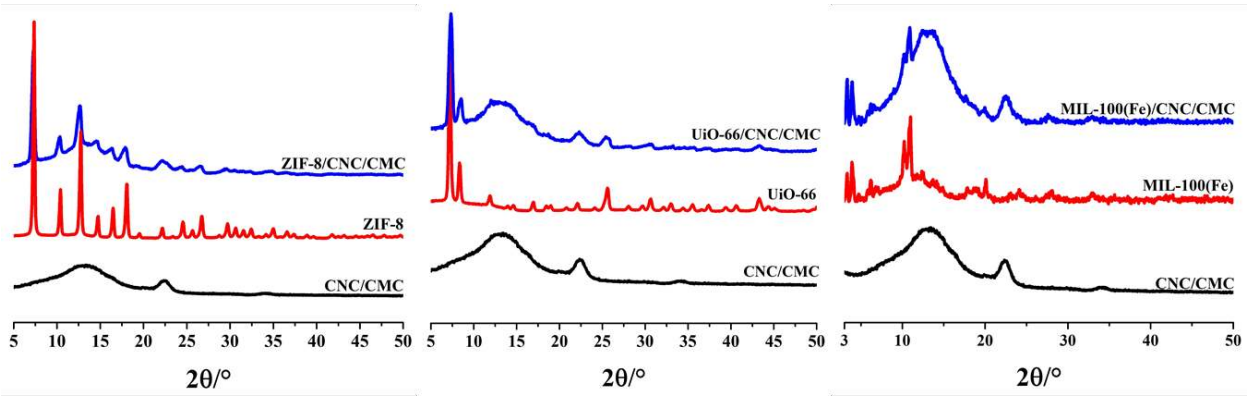

Figure S1. PXRD spectra of a CNC-CMC aerogel, pristine MOFs, and MOF-containing CNC-CMC aerogels.

Table S1. Nominal and measured weight percentage of UiO-66 within aerogels as determined by TGA.

	UiO-66-containing CNC-CMC aerogels[a]		
Nominal mass	20%	33.3%	50%
Ash content	10.46%	15.27%	22.05%
Measured mass	20.86%	33.41%	51.10%

[a] Ash content of plain CNC-CMC aerogel and UiO-66 powders are 2.465% and 40.79% after TGA testing.

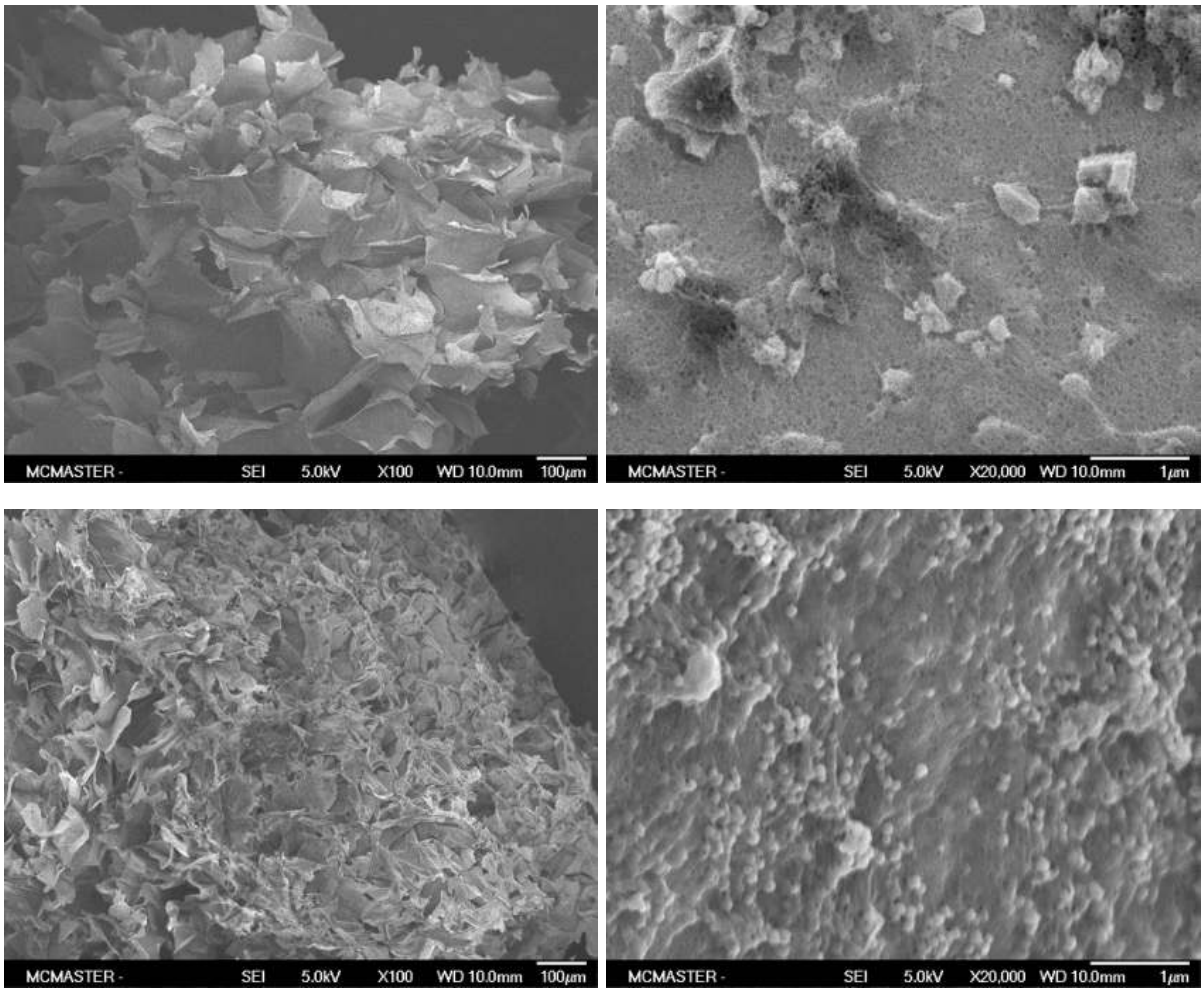

Figure S2. SEM images of ZIF-8 and MIL-100(Fe)-containing aerogels. Upper two images are aerogels with 33.3 wt.% MIL-100(Fe) at different magnifications. Lower two images are aerogels with 40 wt.% ZIF-8 at different magnifications.

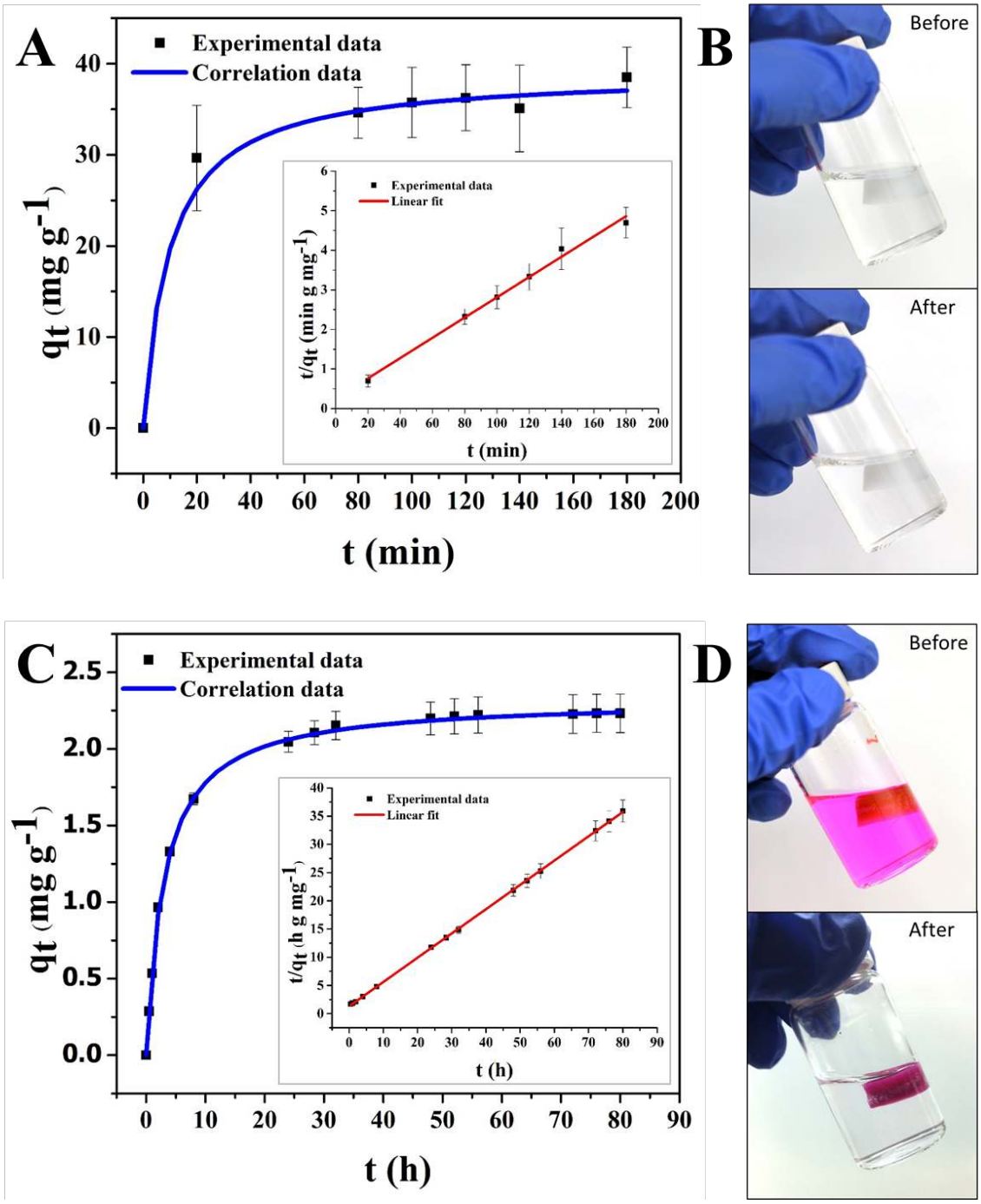

Figure S3. Time dependent adsorption (correlation curve was drawn using the kinetic parameters calculated from the pseudo-second-order model), pseudo-second-order plots (inset) and photographs of the contaminated aqueous solution before and after adsorption of (A, B) benzotriazole on ZIF-8 (40 wt.%) aerogel, (C, D) Rhodamine B on MIL-100(Fe) (33.3 wt.%) aerogel.

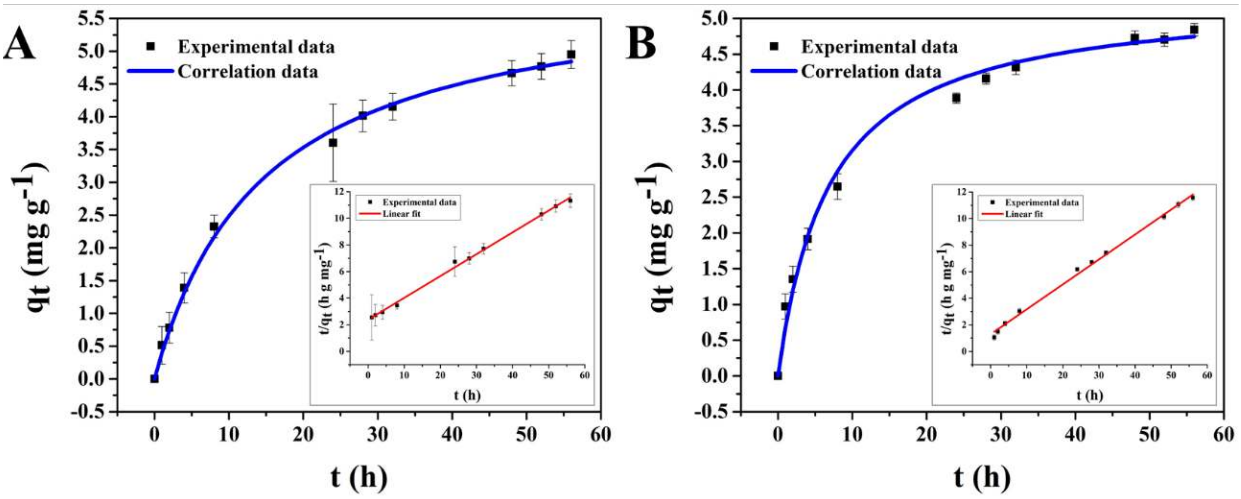

Figure S4. Time dependent adsorption (correlation curve was drawn using the kinetic parameters calculated from the pseudo-second-order model) and pseudo-second-order plots (inset) of the contaminated aqueous solution before and after absorption of Cr(VI) on (A) 20 wt.%, (B) 33.3 wt% loaded UiO-66 aerogel.

Table S2. Kinetic parameters for the adsorption of contaminants (Cr(VI) for UiO-66, benzotriazole for ZIF-8, Rodamine B for MIL-100(Fe)) on MOF loaded aerogels.

		Kinetic parameters		
	MOF loading	$q_{(e)cal}$ (mg g^{-1})	k_2 (g mg^{-1} h^{-1})	R^2
UiO-66	20 wt.%	6.1	0.01	0.9971
	33.3 wt.%	5.33	0.03	0.9963
	50 wt.%	3.91	0.07	0.9990
ZIF-8	40 wt.%	39.06	0.16	0.9927
MIL-100(Fe)	33.3 wt.%	2.32	0.14	0.9999

Table S3. Zr concentration detected by ICP-OES on pure water and water after treated with 50 wt.% loaded UiO-66 aerogel.

	Pure Water	Pure Water after hydrogel compression[a]	Cr(VI) water after hydrogel adsorption[b]
Zr concentration (ppm)	0.077	0.076	0.076

[a] Water was obtained after compression of the 50 wt.% loaded UiO-66 aerogel showed in Supporting Information Video S1. [b] Cr(VI) water was obtained after soaking with 50 wt.% loaded UiO-66 aerogel for 24 hours.